UCRL-JC-133402
PREPRINT

Analysis of Compression Behavior of a [011] TA Single Crystal with Orientation Imaging Microscopy and Crystal Plasticity

A.J. Schwartz
J.S. Stölken
W.E. King
G.H. Campbell
D.H. Lassila
S. Sun
B.L. Adams

This paper was prepared for submittal to the
Materials Research Society 1998 Fall Meeting
Boston, MA
November 30 -December 4, 1998

February 3, 1999

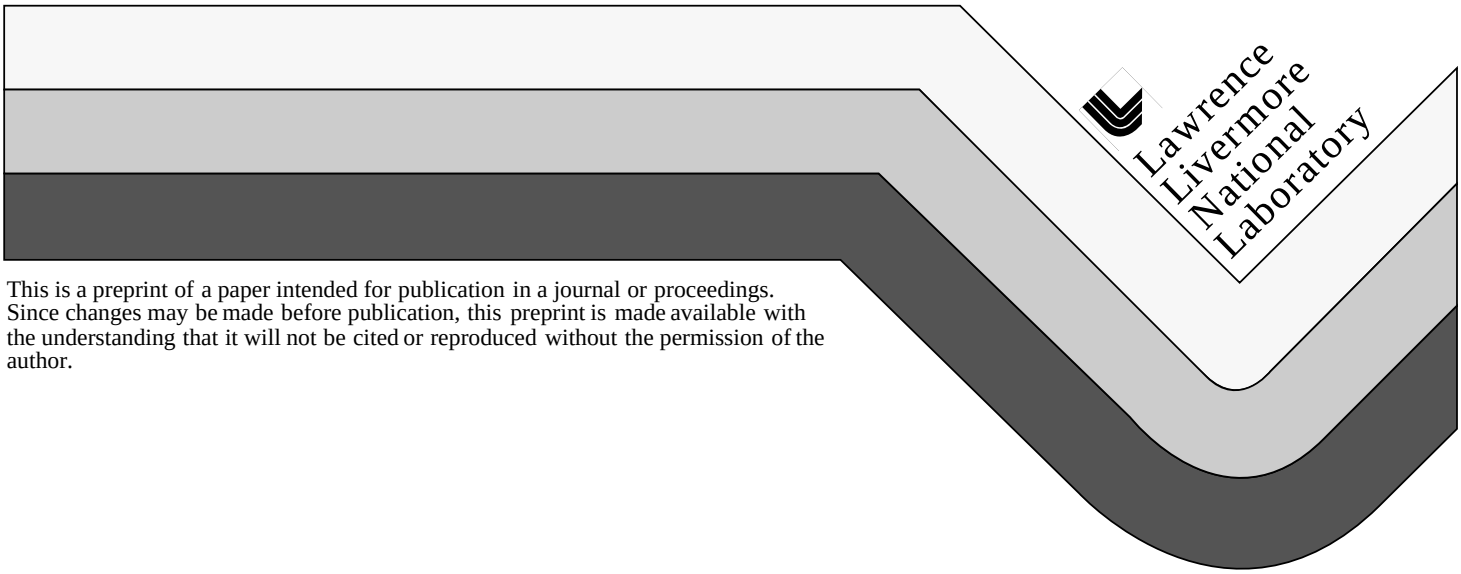

This is a preprint of a paper intended for publication in a journal or proceedings. Since changes may be made before publication, this preprint is made available with the understanding that it will not be cited or reproduced without the permission of the author.

DISCLAIMER

This document was prepared as an account of work sponsored by an agency of the United States Government. Neither the United States Government nor the University of California nor any of their employees, makes any warranty, express or implied, or assumes any legal liability or responsibility for the accuracy, completeness, or usefulness of any information, apparatus, product, or process disclosed, or represents that its use would not infringe privately owned rights. Reference herein to any specific commercial product, process, or service by trade name, trademark, manufacturer, or otherwise, does not necessarily constitute or imply its endorsement, recommendation, or favoring by the United States Government or the University of California. The views and opinions of authors expressed herein do not necessarily state or reflect those of the United States Government or the University of California, and shall not be used for advertising or product endorsement purposes.

ANALYSIS OF COMPRESSION BEHAVIOR OF A [011] TA SINGLE CRYSTAL WITH ORIENTATION IMAGING MICROSCOPY AND CRYSTAL PLASTICITY

A.J. SCHWARTZ, J.S. STÖLKEN, W.E. KING, G.H. CAMPBELL, D.H. LASSILA, J.Y. SHU, S. SUN*, AND B.L. ADAMS*
Lawrence Livermore National Laboratory, Materials Science and Technology Division, Livermore, CA 94550, ajschwartz@llnl.gov
* Materials Science and Engineering Department, Carnegie Mellon University, Pittsburgh, PA 15213

ABSTRACT

High-purity tantalum single crystal cylinders oriented with [011] parallel to the cylinder axis were deformed 10, 20, and 30 percent in compression. The engineering stress-strain curve exhibited an up-turn at strains greater than ~20% while the samples took on an ellipsoidal shape during testing, elongated along the [100] direction with almost no dimensional change along $[0\bar{1}1]$. Two orthogonal planes were selected for characterization using Orientation Imaging Microscopy (OIM): one plane containing [100] and [011] (longitudinal) and the other in the plane containing $[0\bar{1}1]$ and [011] (transverse). OIM revealed patterns of alternating crystal rotations that develop as a function of strain and exhibit evolving length scales. The spacing and magnitude of these alternating misorientations increases in number density and decreases in spacing with increasing strain. Classical crystal plasticity calculations were performed to simulate the effects of compression deformation with and without the presence of friction. The calculated stress-strain response, local lattice reorientations, and specimen shape are compared with experiment.

INTRODUCTION

Ideally, any stress-strain behavior during constitutive testing should be solely a function of the applied (macroscopic) deformation, sample history, orientation, temperature, and strain-rate. In compression tests, "extrinsic" factors such as sample alignment and platen friction augment the "intrinsic" factors [1]. Although the use of tensile specimens largely mitigates the "extrinsic" factors, the convenience and utility of compression specimens can outweigh the disadvantages. This is particularly true for latent hardening tests, in which a sequential set of single slip tests quantifies the constitutive response of a previously inactive slip system as a function of prior slip on another system. The combined intrinsic and extrinsic factors manifest themselves in the evolution of the crystal orientation with strain, which is ideally studied using Orientation Imaging Microscopy (OIM).

OIM is a SEM-based technique that has been primarily applied for characterization of the microtexture of polycrystalline materials [2]. In this method, orientation data at resolutions ≈ 1 μm can be acquired as a function of position on a planar-section. In this investigation, OIM is applied to study the evolution of crystal rotations occurring during compression testing of Ta single crystals and to correlate these results with measured constitutive response. These data provide insight into deformation mechanisms as well as a means to assess the influence of sample geometry and testing conditions on the measured constitutive response. For example, the inhomogeneous stress state in compression specimens arising from platen friction was reported by Cook and Larke to cause anomalous stress-strain behavior [3].

The compression specimens characterized in this work using OIM are of a configuration similar to the second-stage of a latent hardening experiment using typical engineering practice: ~ 1:1 aspect ratio (diameter/height), polished diameter, lapped end-surfaces, and specimen end-surfaces lubricated with a single application of directional polytetrafluoroethylene (PTFE) tape [4]. Tests under these conditions establish a baseline for comparison with the results of more sophisticated, and expensive, experimental techniques such as renewing the solid lubricant at regular intervals during the test and optimizing the type and thickness of lubricant. Ultimately,

the minimization of frictional effects will increase the accuracy of extrapolation methods as described by Ray and Mallik [5] and Singh and Padmanabhan [6] for end-effect correction and decrease the effort in their application.

A unique feature of deformation along the <011> axis of BCC metals is the stable, essentially plain-strain condition that persists to large strains. Compression along the [011] direction results in extension along the longitudinal [100] direction and very small elongation (<1%) along the transverse $\left[0\bar{1}1\right]$ direction. Cylindrical samples take on an ovoid shape within the (011) plane. Hosford [7] has observed similar deformations in the study of drawn BCC polycrystalline <011> textured wires that were first studied in the early 1960's. The origin of this planar deformation mode in single crystals is associated with the fact that the slip directions of all the potentially active {110} and {112} slip planes are contained in a single {110} plane. For the [011] loading direction, the potentially active {110} and {112} slip planes occur in symmetric pairs; each pair contains both $\left[\bar{1}11\right]$ and [111] slip directions. This limits the plastic deformation for [011] loading to the $\left(0\bar{1}1\right)$ plane.

The two-dimensional nature of the plastic deformation is an important consideration in assessing the influence of platen friction on the measured stress-strain response. Simple estimates to account for friction during compression testing have been available for over 70 years [3,8]; however, most of these have assumed axisymmetric deformation. Only since the 1960's have both the necessary experimental methods [9] and theoretical analysis [10,11] been available to examine the influence of friction associated with more complex deformation. These simple analytical methods provide valuable insight and serve as a point of departure for finite-element modeling. A finite-element, crystal-plasticity [12] simulation using a Coulomb friction model of the sample/platen interface is used to study the effects of friction on the nominally homogeneous deformation.

This paper describes the details of crystal growth, purification, specimen preparation, and mechanical testing. The OIM results, discussion of the finite element modeling, and overall conclusions are then given.

EXPERIMENT

Single Crystal Preparation

The single crystal of Ta was grown at the Institute for Solid State Physics in Chernogolovka, Russia, from high-purity stock material provided by Cabot Corporation. The stock Ta was further purified by zone refining in high vacuum. The molten zone was formed by electron beam heating from an annular electrode and five passes through the crystal were taken, with the last pass seeded for growth along [013]. The resultant crystal was 18 mm in diameter and approximately 200-mm in length. Each slice for compression testing was oriented using Laue back-reflection x-ray diffraction. After alignment on the Laue camera, the sample and mounting fixture were transferred as a single unit for sectioning slices approximately 5.1 mm thick by wire electrical discharge machining (WEDM). Compression cylinders approximately 5.47 mm diameter by 4.65 mm length were cut by WEDM from the single crystal disks, then machine turned to near final length and diameter. The diameters were polished with 1200 grit SiC paper followed by Super Blau metallputz paste. The ends were lapped flat and parallel using 1200-grit paper to within 0.01 mm.

Purification Treatment of Mechanical Test Specimens

Impurities in BCC metals are known to have a strong effect on mechanical properties. In Ta, the effects of both substitutional [13] and interstitial impurities [14] have been well characterized. The zone refining steps prior to the single crystal growth allow impurities to volatilize into the vacuum or be swept to one end of the boule. Chemical analysis by glow discharge mass spectrometry shows this method was effective in reducing the concentration of substitutional impurities. A typical analysis reveals Nb and W to be the impurities with highest concentration,

125 and 45 ppmw, respectively. The other impurities include Mo and Re, both at approximately 2 ppmw, while all other substitutional impurities are well below 1 ppmw. These levels of substitutional impurities are not expected to exert a significant effect on the mechanical behavior.

The relevant interstitial impurities in Ta are H, C, N, and O. At levels of a few tens of ppmw, these impurities cause significant increases in both the yield and flow stresses. However, Smialek and Mitchell [14] have demonstrated that these impurities can be removed to below this level by applying an appropriate heat treatment. As the last step in the preparation of mechanical-test specimens, the samples were introduced into an ultra–high vacuum chamber as shown in Figure 1 (a base pressure of $<1 \times 10^{-10}$ torr in the main chamber, but approximately a decade higher at the specimen position). The samples were suspended with a wire of Ta-10%W and were heated by inductive coupling to an external RF coil. The samples were first heated to 1800°C during which most of the dissolved H outgassed from the specimen and was pumped away. Oxygen was then introduced to the chamber to achieve a pressure of 2×10^{-6} torr in order to react with C at the surface of the sample and remove it as CO. The sample was held in this condition for 8 h, after which the oxygen flow was stopped and the temperature of the sample was raised to 2600°C. The high temperature treatment removed O and N from the sample as observed in the vacuum by residual gas analysis. Two of the mechanical test specimens were held for 8 h while a third one was held for 18 h. At the end of the longer time at high temperature, the vacuum in the chamber fully recovered to its base pressure level. Upon removal of the specimens from the vacuum chamber, they were immediately placed into a dewar of liquid nitrogen in order to slow the kinetics of re–introduction of any impurities. The purity of the specimens was characterized by measuring their electrical resistivity at room temperature and at slightly above the Ta superconducting transition temperature at 4.5K. The residual resistivity ratios achieved are in the range of 700 for the short-time anneal and 1500 for the longer time. Prior to mechanical testing the samples are warmed to room temperature in ethyl alcohol.

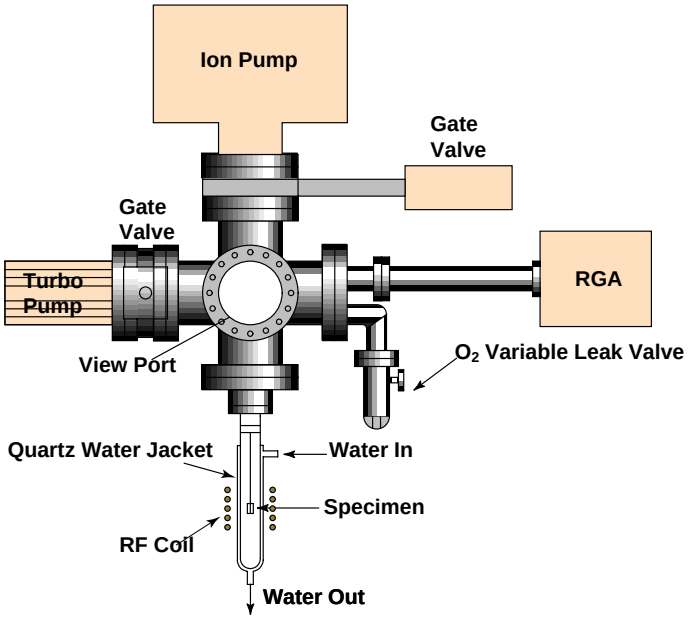

Figure 1. Schematic of purification apparatus.

Mechanical Testing

A series of mechanical tests aimed at understanding the deformation behavior of high-purity tantalum single crystals was undertaken. Quasistatic compression tests were performed in a subpress with tungsten carbide platens using an Instron 1127 short frame test machine and an MTS 7.6-mm extensometer was used to measure the relative motion of the platens. Teflon tape

was pre-loaded to 2045 kg for use as a lubricant. All of the results described here pertain to samples tested at room temperature at a strain rate of $10^{-3}\,s^{-1}$.

The engineering stress - engineering strain response of three [011] single crystal compression samples is shown in Figure 2. These purified specimens exhibit a minor yield drop, followed by a nearly linear region of hardening. At approximately 20% engineering strain, the stress - strain response begins to turn up. This is due to a combination of the non-linearity of engineering strain and the effects of platen friction.

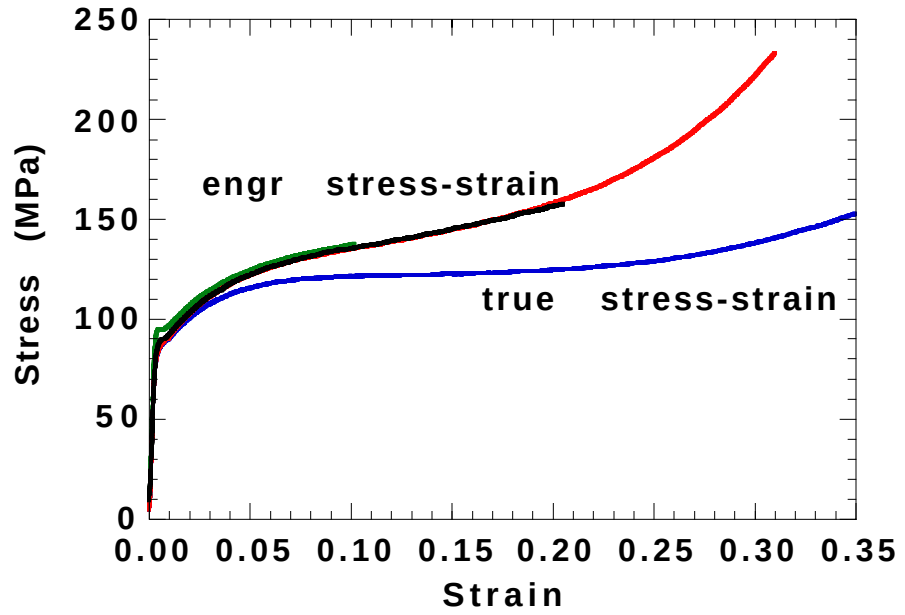

Figure 2. Room temperature stress-strain response of high-purity Ta [011] single crystals at a strain rate of $10^{-3}s^{-1}$.

Orientation Imaging Microscopy

The objective of the OIM analysis was to explore the variations in local lattice rotations as a function of position in the sample for several strains. The ovoid samples were sectioned along the plane containing [011] and [100] to reveal the longitudinal view. The unused half was sectioned again to reveal the transverse plane, which contains $\left[0\bar{1}1\right]$ and [011]. These specimens were mounted in conductive epoxy and prepared for OIM examination using standard lapping procedures.

The OIM technique is based on automatic indexing of the backscatter Kikuchi diffraction patterns within a scanning electron microscope. Individual orientation measurements are made at discrete points on the sample, defined on a grid. At each point during the scan, the orientation is recorded along with coordinates describing the position. Images (or maps) can be generated by mapping the crystal orientation (or misorientation) onto a color or grayscale and shading each point on the grid according to some aspect of the crystal orientation. Up to five individual OIM scans were required to cover the longitudinal section and two for the transverse section. Each individual scan was analyzed separately and plotted in terms of in-plane and out-of-plane rotation angles. These overlapping maps were then aligned to assemble an overall collage.

To examine local lattice rotations, the Euler angles relative to a reference orientation at the section center are decomposed to their in-plane and out-of-plane components. The in-plane and out-of-plane crystal-rotation maps for all three compression tests reveal inhomogeneous deformation everywhere and particularly large lattice rotations in the corners of the longitudinal section.

RESULTS

Figure 3 illustrates the measured lattice rotations of the [011] specimen compressed 10% with a misorientation scale of 0 to 5 degrees. These three scans have step sizes between 13 and 15 microns. The existence of features in the crystal rotation field with sizes on the order of the step size will be observed as single points in the OIM scan, however, their morphology will not be resolved. In the longitudinal plane, rather sharp changes in crystal orientation (~1°) are observed that appear to be geometric in nature and emanate at approximately 45° from the top and bottom corners. These features, which do not appear to correspond to the traces of either the {110} or {112} slip planes, or <111> slip directions, appear early in deformation and persist throughout. A second type of contrast feature lying roughly perpendicular to the above features is observed which is characterized by relatively smaller changes in orientation (~0.5°). Of particular interest are the alternating orientation changes observed upon crossing several of these features. This suggests the existence of networks of dislocations with net alternating sign that are required to accommodate the observed rotations. Essentially all of the rotations measured with OIM are about the $[0\bar{1}1]$ axis, i.e. no significant lattice rotations occur out of the $(0\bar{1}1)$ plane. This is consistent with the Burgers vectors being contained in the observed section. These common features are observed in all of the specimens studied.

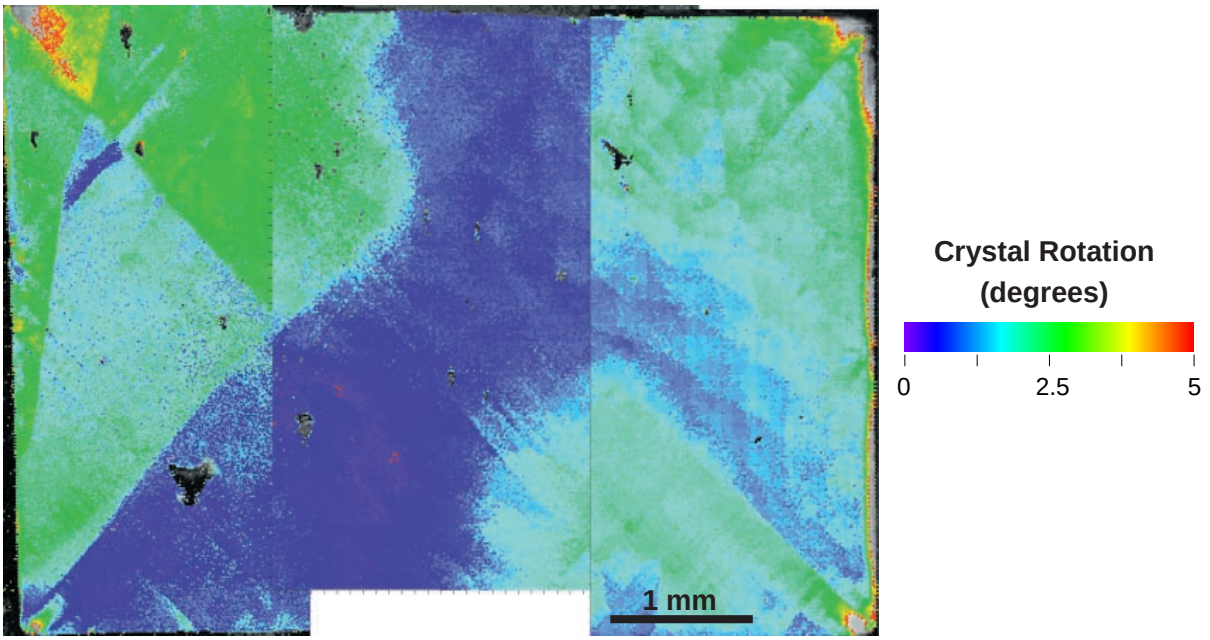

Figure 3. Misorientation collage of the 10% compressed sample, longitudinal view. Rather sharp changes in crystal orientation (~1°) are observed that appear to be geometric in nature and emanate at 45° from the top and bottom corners.

Figure 4 represents a collage of the four scans required to cover the 20% compressed specimen plotted on the misorientation scale from 0 to 10 degrees. The rotations are all about the $[0\bar{1}1]$ axis with the largest lattice rotations occurring in the corners and prominent misorientation features emanating from the corners. The finer-scale contrast features normal to these are more pronounced than the 10% compressed specimen. In addition, the spacing of these alternating misorientations is smaller.

Figure 5 reveals the longitudinal section of all but the 300 micron wide region on the right side of the specimen compressed 30%. This image spans a misorientation scale from 0 to 15 degrees. Rotations greater than 15 degree occur in the corners as well as at the ends of the horizontal midplane. Abrupt orientation changes are observed throughout this figure. Of particular interest is the approximately 5 degree alternating misorientations with width on the

order of 70 microns. The spacing, magnitude, and angles of the alternating misorientations are observed to increase in number density and decrease in spacing with strain. Specifically, at 10% compression, the angle between primary bands is approximately 95 degrees. This decreases to 85 then 80 degrees as the specimen is compressed to 20% and 30% deformation, respectively [15]. Observed rotations are about the $[0\bar{1}1]$ axis.

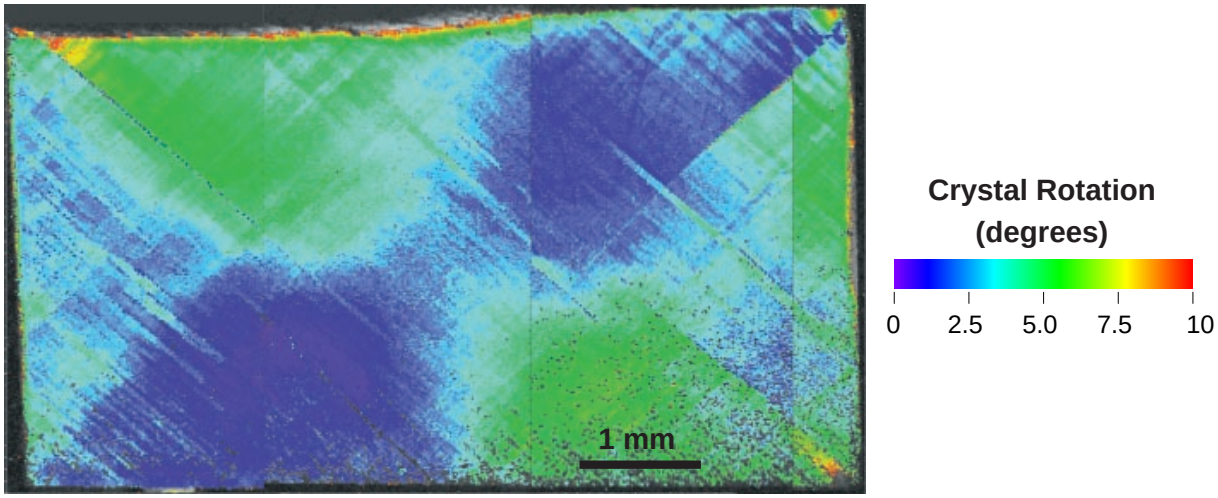

Figure 4. Misorientation collage of the 20% compressed sample, longitudinal view. The rotations are all about the $[0\bar{1}1]$ axis with the largest lattice rotations occurring in the corners and prominent misorientation features emanating from the corners.

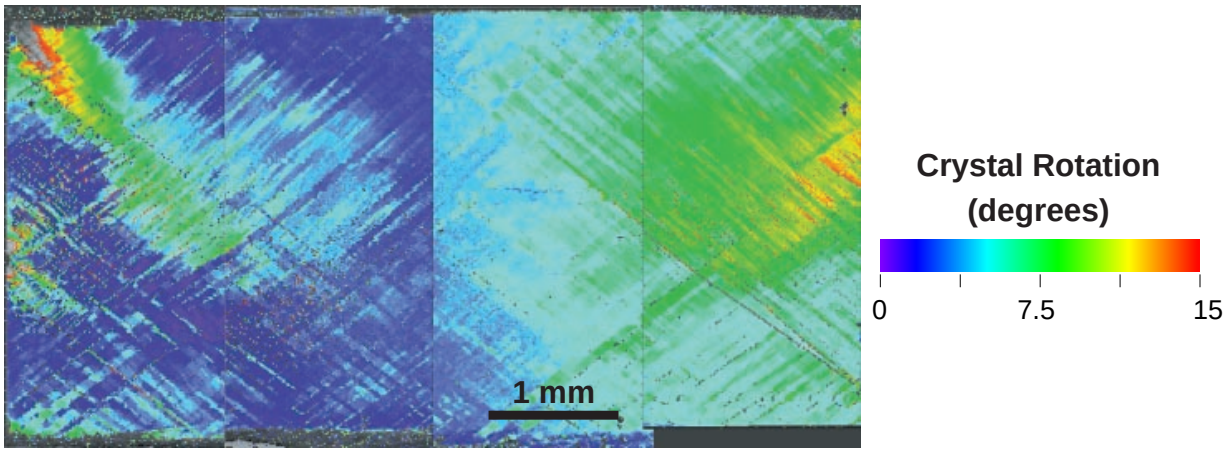

Figure 5. Misorientation collage of the 30% compressed sample, longitudinal view. Greater than 15 degree rotations occur in the corners as well as at the ends of the horizontal midplane. Severe orientation changes are observed throughout this figure. Of particular interest is the approximately 5 degree alternating misorientations with width on the order of 70 microns. Observed rotations are about the $[0\bar{1}1]$ axis.

Figure 6 is a higher resolution OIM image of the specimen compressed 20% and suggests that the bands discussed above are discrete ~2 to 5 μm wide regions of relatively large rotations. These bands are aligned approximately 85° with respect to each other but do not lie along the traces of the slip planes. Rotations as large as 5° are observed within the bands while the intersection causes a displacement across the band.

Rotation maps from the transverse section shown in Figure 7 are distinctly different in appearance from those in the longitudinal plane. Figure 7(a) is a low-resolution scan with step size equal 16 μm and scans one-half of the transverse section from the top to the bottom. Figure 7 (b) reveals the out-of-plane rotations with 1 μm step size resolution. The features of these out-of-plane rotation maps are neither as sharp nor as straight as those observed in the longitudinal section. The rotation maps confirm that the rotations observed are about the $[0\bar{1}1]$ axis suggesting the importance of slip on the {112}<111> slip systems. Alternating orientation changes are also observed on this section. Features likely corresponding to the 2 to 5 μm wide bands of Fig. 6 are observed in Fig. 7b.

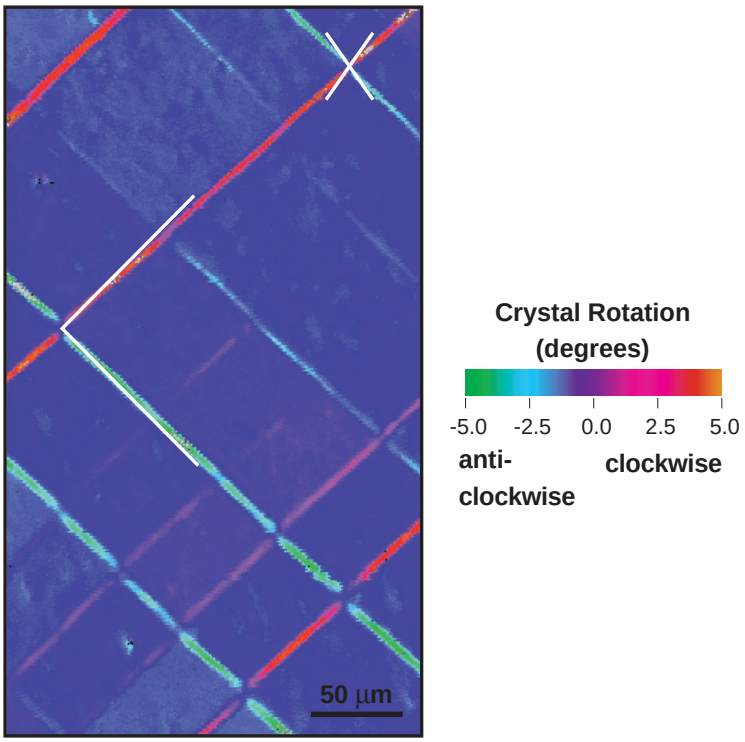

Figure 6. High magnification OIM image of the specimen compressed 20%. Orthogonal lines in the center show that the bands intersect at an angle < 90°. Oblique lines at the top right are the traces of the {110} and {112} slip planes in the longitudinal section.

DISCUSSION

The upturn in the stress-strain diagram above 20% strain is similar to that seen by numerous other investigators [1,3-6] during compression testing; however, the effect seems particularly acute. The magnitude of the upturn and its occurrence at relatively low strain suggests that factors other than friction may be significant. A two-step approach shall be used to assess the impact of platen friction on the deformation. First, using simple analytical models, the frictional contribution to the flow stress shall be estimated. The resulting parameters shall then be used as input to a finite element simulation to gage the effect of friction on lattice rotations.

One of the first published estimates of the influence of platen friction on the measured flow stress during compression testing is due to Siebel [8]:

$$\sigma_{obs}/\sigma_{flow} = 1 + C\ (d/h), \qquad (1)$$

where σ_{obs} is the observed flow stress, σ_{flow} is the true flow stress measured under uniform deformation, d is the sample diameter, h is the sample height, and C is a constant.

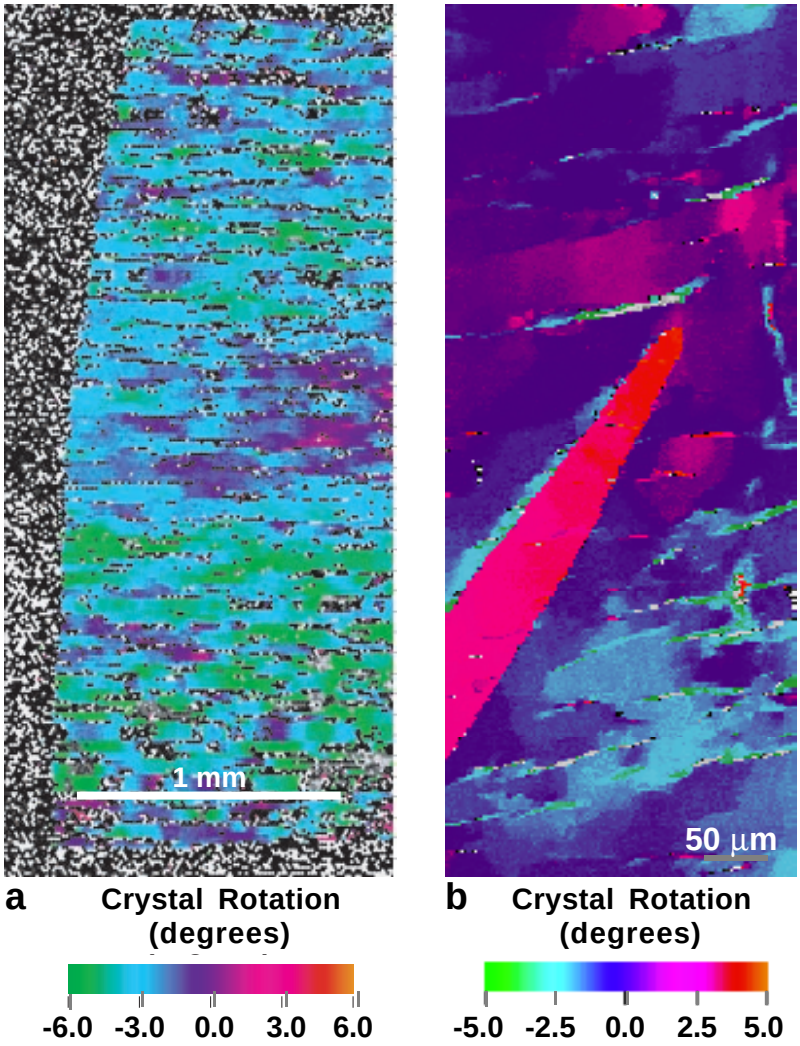

Figure 7. Misorientation maps of the 30% compressed sample, transverse view. The features of these out-of-plane rotation maps are neither sharp nor straight. The rotation maps confirm that the rotations observed are about the $[0\bar{1}1]$ axis suggesting the importance of slip on the {112}<111> slip systems. Alternating orientation changes are also observed on this section. (a) low resolution, 16.0 μm step size scan, (b) high resolution, 2.0 μm step size scan.

Using the Tresca yield criterion and flow rule, the value of C is μ/3, where μ is Coulomb's coefficient of friction equal to the tangent friction force divided by the normal force. Although Eqn. 1 is predicated on small values of C, its applicability is quite broad since it was shown by Avitzur [16] to be identical to the upper-bound solution for the compression of a cylinder between two rigid dies. In both cases the deformation is considered to be axisymmetric. Using a generalized Galerkin method, Hill [10] considered the compression of an arbitrary cross-section for both two- and three-dimensional deformations, obtaining:

$$C = \mu/3 \quad \text{(in 3D)} \qquad (2)$$

$$C = \mu/2 \quad \text{(in 2D)} \qquad (3)$$

These relations were later rederived by Collins [11] using an upper-bounds technique. Thus for a given (d/h), frictional effects under 2D deformation are 50% greater than those in the 3D case, at least to first order in μ. This is consistent with the enhanced upturn observed during the essentially plane-strain compression of the [011] oriented single crystal.

The earlier occurrence of the upturn during plain-strain deformation, as compared to the axisymmetric deformations cited in the literature, may be reconciled by considering the

relationships between the applied strain and the sample aspect ratio in both two and three dimensions. For isochoric deformations in 2D it is easily shown that the aspect ratio r (r=d/h) may be written as the following function of the engineering strain (e):

$$r = r_o (1\text{-}e)^{-2} \quad \text{(in 2D)} \tag{4}$$

while in 3D:

$$r = r_o (1\text{-}e)^{-3/2} \quad \text{(in 3D)} \tag{5}$$

For samples with the same initial aspect ratio (r_o), at any given compressive strain (e) the aspect ratio of a sample deforming in 2D is $(1\text{-}e)^{-1/2}$ times greater than that of the 3D case. For an applied strain of 30%, this difference amounts to a 20% increase. For an applied strain of 40%, the change in aspect ratio is 29% greater in 2D than in 3D. The net effect of the larger friction factor (increased C) in 2D coupled with the greater change in aspect ratio for a given strain significantly enhances the influence of friction in 2D deformation as compared to 3D. For an applied strain of 30% the combined increase is 80%, while at 40% strain the overall enhancement of the frictional effect is over 93%.

A simple estimate of the friction coefficient may be derived by assuming a linear hardening relation:

$$\sigma_{low} = \sigma_o + H\,\varepsilon \tag{6}$$

where σ_{flow} is the true flow stress, σ_o is the initial yield stress, H is the hardening rate, and ε is the true strain. This is substituted into Eqn. 1 and solved for the friction factor (C). Assuming that the initial friction is small (μ=0.04) for small strains (<10%), the values of σ_o and H is obtained:

$$\sigma_o = 115 \text{ MPa}, \quad H = 28 \text{ MPa} \tag{7}$$

Using these values, the friction factor is calculated for larger values of strains. In doing so it is observed that the value of C varies monotonically from 0.02 at 10% strain to 0.1 at 30% strain. It should be emphasized that these values of C are highly dependent upon the chosen hardening model, since the measured response is a convolution of friction and hardening. The goal here is two-fold: to show that the apparent rapid hardening rate can be attributed to friction when accounting for the two-dimensional nature of the deformation and to provide a point of departure for finite-element modeling of the deformation. In this spirit, the evolution of friction with deformation is modeled using a simple one-parameter model describing a linear rise in the friction factor with aspect ratio. The corresponding value of μ varies linearly from 0.04 at 0% strain to 0.20 at 30%. These values are consistent with nearly perfect lubrication initially to that typical of lubricated metals [17] at 30% strain. The stress-strain behavior predicted by this model along with the experimental data is shown in Figure 8. A curve showing the behavior in the absence of friction is also shown. Using reasonable values for the model parameters results in an acceptable fit to the experimental data considering this simple model.

The evolution of friction stresses at the sample/platen interface is in general extremely complicated, dependent upon both the material response and lubrication conditions at the interface. This will be investigated in detail in a later series of experiments and simulations; however, the present focus shall be on the initial stages of deformation (<10% strain) where friction is considered constant. In this regime it is of interest to examine the role that friction plays in altering the nominally homogeneous deformation and making comparisons with the OIM observations.

A finite-element simulation of the compression sample was performed using Coulomb friction to model the sample/platen interface and a crystal plasticity [12] constitutive relation to model the specimen. The platens were modeled using isotropic elasticity. A crystal plasticity model similar to that of Kothari and Anand [18] has been implemented in the implicit finite element code Nike3D [19]. The material parameters are chosen to be those used by Kothari and Anand, with the following exceptions. The initial flow stress and hardening rate were selected to be consistent with the above values of σ_o and H for the [011] orientation and linear hardening was assumed.

Independent hardening of the slip systems is used, since extensive latent hardening data are unavailable. Slip on both the {112} and the {110} slip-planes is considered. The coefficient of friction at the sample/platen interface is taken as 0.08, consistent with the above observations. Using these parameters, models of both the entire sample and one-eighth the sample were constructed using 243 and 162 elements, respectively. Since the simulation of the entire specimen essentially duplicated the plane-strain deformation observed in the experiments, we shall focus on the one-eighth of the specimen modeled with 162 elements and three symmetry planes.

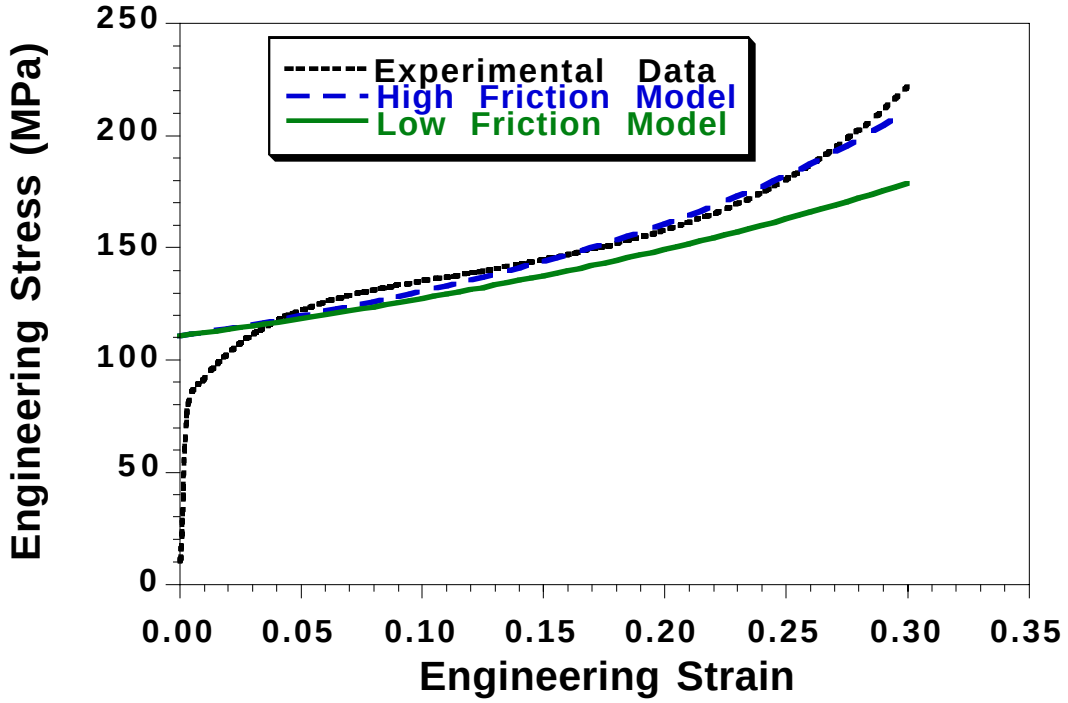

Figure 8. Comparison of the experimental and simulated stress-strain response of the [011] Ta single crystals. Calculations were performed with both low and high friction models and revealed the strong influence of friction on the measured constitutive behavior.

An elementary crystal plasticity calculation [20] indicates that uniaxial compression in BCC metals along the [011] axis in the absence of friction should result in homogenous compression and an associated elongation along the [100] axis. The deformation is contained within the $(0\bar{1}1)$ plane and the lattice rotation is zero. The presence of frictional forces alters this picture, resulting in inhomogeneous deformation and associated crystal rotations.

This can be seen in the finite element simulation shown in Figure 9. For an applied strain of 6%, the lattice rotation in the corner regions is almost two degrees, while the central region of the sample is essentially unrotated. The axis of rotation is parallel to the normal of the plane of the deformation. The deformation and rotations are essentially two-dimensional, even though this is a full three-dimensional calculation. The overall deformation pattern and the magnitude of the lattice rotations are in good agreement with the OIM observations; however, the details of the lattice rotations are not. To explore this further, higher resolution simulations were performed.

In order to reduce the large computational burden of three-dimensional calculations, the two-dimensional nature of the deformation was exploited. A slice of the sample parallel to the longitudinal section was modeled assuming that it deformed in plane strain. This appears to be a good approximation in light of the above experimental observations. In doing so, finely meshed finite-element simulations could be performed in a few days. The mesh size in the corners corresponds to 10 μm, with over 400 elements in the entire model. All other features (constitutive parameters, friction coefficient, etc.) of the model are identical to the previous three-dimensional case. The results of this simulation are shown in Figure 10. The maximum rotation has increased to ~2.3 degrees and the deformation pattern in the corners has become sharper and

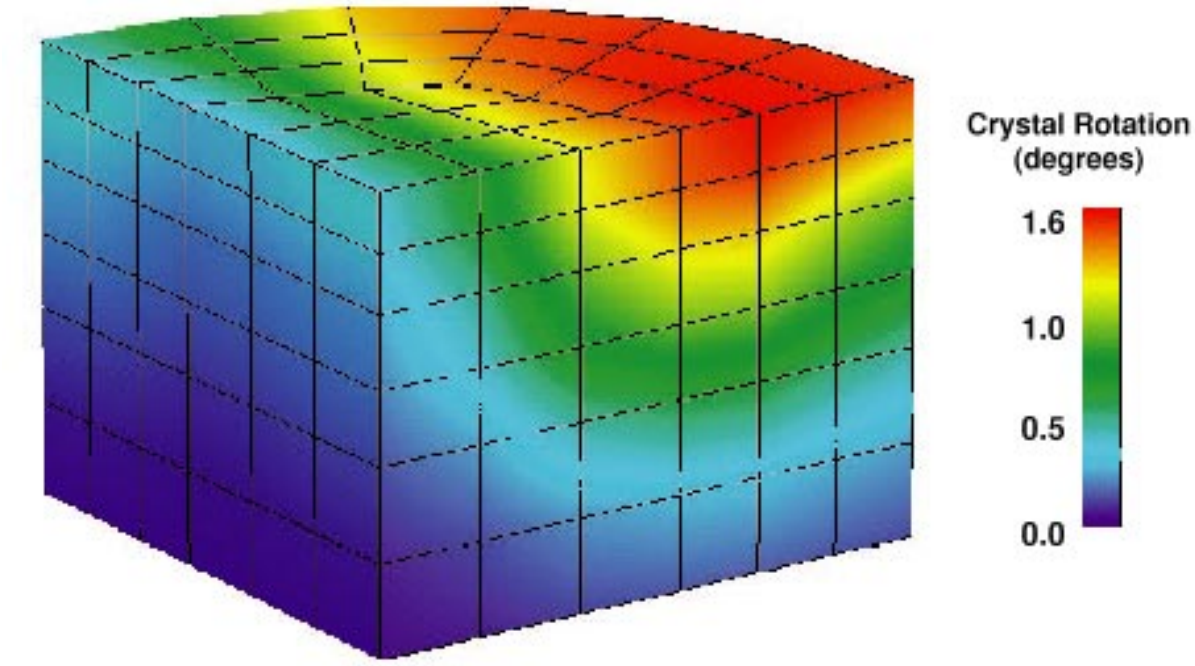

Figure 9. One-eighth section of full three-dimensional finite element simulation of crystal rotations caused by compression deformation with platten friction. Maximum rotations of 1.6 degrees occur in the upper-right corner, while the center remains unrotated. Applied strain: 6%.

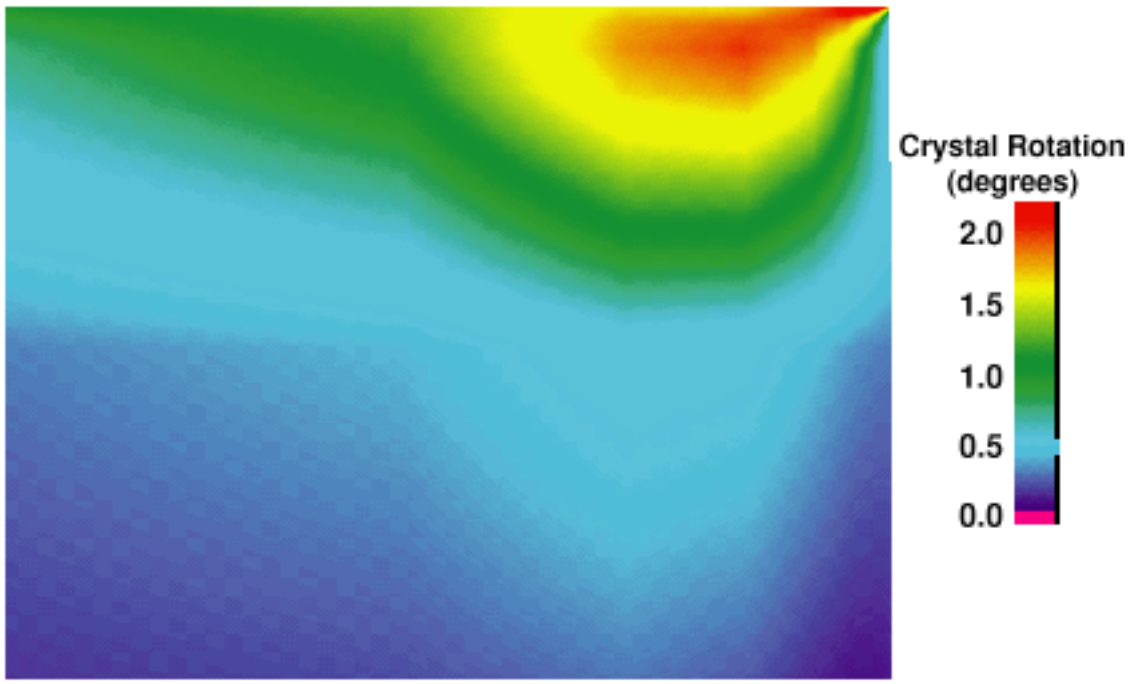

Figure 10. High resolution, finely meshed, plane-strain finite element simulation of crystal rotations caused by compression deformation with platen friction. Maximum rotations of 2.3 degrees occur in the upper-right corner, while the center remains unrotated. Applied strain: 6%.

more well defined. Experimentation with different mesh sizes and the number of elements leads to the conclusion that the finite element solution exhibits the well-known size effect of classical computational plasticity[21], i.e., without a length scale in the plasticity model, the finite element solution is dependent upon the size of the mesh used in the calculation. It is for this reason that higher resolution calculations with even finer meshes have not been employed to examine the rotations observed by OIM at the smallest scale.

CONCLUSIONS

Friction exerts a significant effect in the compression deformation of the [011] single crystals giving rise to an enhancement of the apparent flow stress at strains in excess of 20%. The two dimensional nature of the deformation exacerbates the effects of platen friction. To first order, the enhancement can be explained by frictional effects without invoking crystal plasticity. The macroscopic lattice rotations at small strains (<10%) predicted by finite-element calculations using a Coulomb friction model are in reasonable agreement with OIM observations. Higher order deviations of the experimental results from simple model calculations are likely the consequence of crystal plasticity. Frictional effects drive lattice rotations at the sample corners which likely spawn inhomogeneous bands of deformation throughout the sample. The bands, which are ~2 to 5 μm in width and bounded by low angle boundaries, evolve with strain. The resolution of these fine-scale lattice rotations awaits the implementation of a scale-dependent crystal plasticity formalism needed to remove the mesh dependence of the finite element solution.

The authors thank Mr. Robert K. Kershaw for performing the metallography, and Ms. Mary M. LeBlanc for mechanical testing. This work is performed under the auspices of U.S. Department of Energy and Lawrence Livermore National Laboratory under contract No. W-7405-Eng-48.

REFERENCES

1. T.C. Hsü, Materials Research and Standards, **9**, No. 12, p. 20 (1969).
2. T.A. Mason and B.L. Adams, Journal Of Metals, **46**, No. 10, p. 43 (1994).
3. M. Cook, and E.C. Larke, Journal Inst. Metals, **71**,p. 371, 1945.
4. J.S. Gunsekera, J. Havranek, and M.H. Littlejohn, Journal of Engineering Materials and Technology, **104**, p. 275 (1982).
5. K.K. Ray and A.K. Mallik, Trans. Met. Soc. of AIME, **14A**, p. 155 (1983).
6. A.P. Singh and K.A. Padmanabhan, Journal of Materials Science, **26**, p. 5481 (1991).
7. W.F. Hosford, Jr., Trans. Met. Soc. of AIME, **230**, p. 12 (1964).
8. E. Siebel, and A. Pomp, Kaiser-Wilhelm Inst. EisenForsch, **9**, p. 157 (1927).
9. A.T. Male, and M.G. Cockcroft, Journal Inst. Metals, **93**, p. 38 (1964-65).
10. R. Hill, J. Mechanics and Physics of Solids, **11**, p. 305, (1963).
11. I.F. Collins, J. Mechanics and Physics of Solids, **17**, p. 323, (1969).
12. R.J. Asaro, Advances in Mechanics, **23**, p. 1, (1983).
13. P.L. Raffo, and T.E. Mitchell, Trans. Met. Soc. of AIME, **242**, p. 907 (1968).
14. R.L. Smialek and T.E. Mitchell, Phil. Mag., **22**, p. 1105 (1970).
15. A.J. Schwartz, W. E. King, G. H. Campbell, J. S. Stölken, D. H. Lassila, S. Sun , and B. L. Adams, Accepted, Journal of Engineering Materials and Technology (1998).
16. B. Avitzur, *Metal Forming, Processes and Analysis*, p. 78, McGraw-Hill, NY, (1968).
17. H.H. Ryffel, Ed., *Machinery's Handbook*, 22nd Ed, Industrial Press, NY p. 436 (1984).
18. M. Kothari and L. Anand, J. Mechanics and Physics of Solids, **46**, No 1, p. 51, (1998).
19. B.N. Maker, Nike3D: A nonlinear, implicit, three-dimensional finite element code for solid and structural mechanics - user's manual, LLNL, UCRL-MA-105268 Rev 1, (1995).
20. G.Y. Chin, R.N. Thurston, and E.A. Nesbitt, Trans. Metal. AIME, **236**, p. 69 (1966).
21. A. Acharya, and G. Shawki, J. Mech. and Physics of Solids, **43**, No. 11, p. 1751 (1995).